Theory of paramagnetic singlet-doublet excitations in double-hexagonal close-packed praseodymium*

Per Bak
Brookhaven National Laboratory, Upton, New York 11973
(Received 19 May 1975)

The magnetic excitation spectrum of the singlet-doublet magnet double-hexagonal close-packed praseodymium, which has been measured by means of inelastic neutron scattering, is analyzed using a diagrammatic high-density expansion technique. The lowest-order random-phase-approximation diagrams give a detailed description of the wave-vector and temperature dependence of the four modes in terms of a Hamiltonian including isotropic Heisenberg interatomic exchange interactions and anisotropic, dipolarlike exchange interactions. In general, the modes are linearly or elliptically polarized. The leading contributions to the line shapes of the excitations are obtained by extending the $1/Z$ expansion of the generalized susceptibility propagators one order beyond the random-phase approximation. This damping corresponds to spin-wave scattering on single-site fluctuations. The propagators are calculated self-consistently by including internally renormalized Green's functions. The theoretical spectral functions are in detailed agreement with experiment.

I. INTRODUCTION

For the last several years there has been a great interest in the properties of localized magnetic systems which possess a nonmagnetic singlet ground state.[1] The ordering in such systems occurs as an exchange polarization of the ground state, provided the exchange interaction between the magnetic ions exceeds a certain threshold value. Double-hexagonal close-packed (dhcp) praseodymium is an example of a singlet-ground-state magnet in which the exchange is only slightly undercritical with respect to magnetic ordering.[2]

In the double-hexagonal close-packed structure with stacking sequence $ABAC$, the Pr ions experience a crystal field of cubic symmetry at the A sites and of local hexagonal symmetry at the B sites. The atomic ground state is the ninefold degenerate $^3H_4$ multiplet. Magnetization measurements,[3] as well as neutron-scattering experiments[2,4,5] clearly demonstrate that the resulting crystal-field ground state on the hexagonal sites is the pure $|J^z=0\rangle$ singlet, and the first excited state is the doublet $|x\rangle$, $|y\rangle$, where $|x\rangle=(1/\sqrt{2})(|1\rangle+|-1\rangle)$ and $|y\rangle=-(i/\sqrt{2})(|1\rangle-|-1\rangle)$. The paramagnetic excitation spectrum arises from the transitions between these states, coupled together by the interatomic exchange interaction. Hence, the hexagonal ions constitute an effective spin-1 system with uniaxial anisotropy, if the higher excited states are neglected.

The spin dynamics has recently been measured by Houmann *et al.*[2] using inelastic-neutron-scattering techniques. dhcp praseodymium seems to be the simplest real singlet-ground-state magnet, and significantly more information is now available on the excitations in this material than in any other paramagnetic system. This makes the element Pr almost ideal for a confrontation between experiment and theoretical model calculations. A preliminary analysis of the spectrum[2] showed that anisotropic two-ion interactions are important, as could be expected from spin-wave studies of the heavy-rare-earth elements.[6,33] Moreover, the temperature dependence of the excitation energies were found to be in substantial agreement with a random-phase theory (RPA), in apparent contrast to neutron-scattering results for the singlet-ground-state magnet Pr_3Tl.[7] The lowest-lying mode shows a clear tendency towards softening as the temperature is lowered towards 0 K, but no critical effects were observed. However, antiferromagnetic ordering corresponding to this mode has been observed in a single crystal of Pr with 3-at.% Nd.[8] In addition to the strong temperature dependence of the exciton energies, a dramatic increase of the intrinsic linewidth was observed as the temperature was raised from 6 to 30 K, where well-defined modes cease to exist.

Most of the theoretical work on singlet-ground-state systems has been based on the random-phase approximation (RPA) using a variety of different representations of the single-ion states,[9–13] or on pseudoboson theories,[14–16] which essentially give the zero-temperature limit of the RPA. More elaborate theories[17,18] based on various higher-order decouplings of equations of motions of spin operators give corrections to the exciton energies. However, inconsistencies and ambiguities are introduced through the decoupling procedures as already pointed out by Murao and Matsubara[19] and it is difficult to estimate the errors introduced via the truncations. Another shortcoming of these theories is that they give infinite lifetimes of the excitations and thus completely neglect damping effects.

Another approach to the calculation of correlation functions in the paramagnetic regime is the method of Blume and Hubbard,[20] which has been applied to

the transverse Ising model (or singlet-singlet system) by Moore and Williams.[21] This approximation may be superior at high temperatures. Common to all the above-mentioned approaches is the lack of well-defined expansion parameters, which greatly precludes systematic calculations. An alternative type of theory is the diagrammatic Green's-function expansion method developed by Vaks, Larkin, and Pikin[22] (VLP) for spin operators to calculate correlation functions to any order of perturbation theory. The formalism has later been generalized by Kashchenko *et al.*,[23] and by Izyumov and Kassan-Ogly.[24] Yang and Wang[25] extended the method to any multilevel magnetic system using a standard basis operator representation. This representation has previously been used, within the random-phase approximation, by Haley and Erdös[26] in the discussion of a spin-1 system, and by Purwins *et al.*[27] and by Bak[28] in the analysis of magnetic excitations and excited-state spin waves in real multilevel systems.

The VLP formalism corresponds to the semi-invariant theory introduced by Stinchcombe *et al.*,[29] which has been applied to the Ising model in a transverse field.[30] In contrast to the other techniques, this kind of theory gives a well-defined high-density expansion parameter $1/Z$ or $1/r_0^3$, allowing us to perform systematic self-consistent calculations, and to recognize the physical processes involved. Z is an effective number of ions interacting with a given ion, and r_0 is an effective interaction length defined by Vaks *et al.*[22] The approximations are now based on physical, not technical reasons. Only in the critical regime, or in an overdamped situation, the formalism is inadequate to any order in $1/Z$, but this restriction is not relevant to Pr, since this material is paramagnetic at any temperature. The rapid $\vec{q}$ dependence of the measured excitation energies (Fig. 1) shows that the forces are of long range, indicating that the high-density expansion is applicable. As is well known, the zeroth-order terms provide the magnetization in the mean-field approximation and the RPA theory for the correlation functions. Encouraged by the success of the RPA in describing the temperature dependence of the exciton energies,[2] we may hope that inclusion of higher-order terms in the $1/Z$ expansion give a good description of damping effects and hence the complete spectral function of the excitations as measured by inelastic neutron scattering.

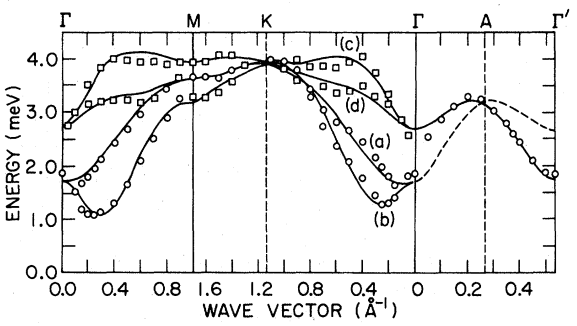

FIG. 1. Dispersion relations for magnetic excitations propagating on the hexagonal sites in dhcp praseodymium. The experimental data are taken from Ref. 2. The squares and the circles denote modes measured to be dominantly of optical, and dominantly of acoustic nature, respectively. In general, the lower optical and acoustic branches are polarized along the $\vec{q}$ direction and the upper branches perpendicular to $\vec{q}$. The full lines represent a least-squares fit as described in the text.

Section II presents the Green's-function formalism to be used in this paper and the low-temperature dispersion relations are analyzed within the RPA. The nature of the different modes is discussed in terms of the spin correlation functions, which are closely related to the Green's functions. In general, the modes are linearly or elliptically polarized. The analysis enables us to set up a complete model Hamiltonian for Pr. In principle, we can then perform numerical calculations of correlation functions and other thermodynamical quantities to any order at any temperature without introducing further adjustable parameters, the only restriction being the limited computer capacity. In Sec. III, the complete spectral function is calculated at several temperatures and energies by extending the $1/Z$ expansion one order beyond the random-phase approximation. The calculation is performed self-consistently, taking into account internally renormalized propagators. The theoretical line shapes are in substantial agreement with experiment.

In Sec. IV the significance of the results will be discussed with emphasis on the implications for other magnetic and nonmagnetic multilevel systems, and further experiments are suggested.

II. RPA THEORY

The Hamiltonian describing the magnetic properties of the Pr ions at the hexagonal sites may be written as the sum of a single-ion term $\mathcal{H}_0'$ and a two-ion exchange term $\mathcal{H}_1'$, where

$$\mathcal{H}_0' = \sum_i V_{ci} , \tag{1a}$$

$$\mathcal{H}_1' = -\sum_{ij} \sum_{lml'm'} \mathcal{K}_{ll'}^{mm'}(\vec{r}_i - \vec{r}_j) O_l^m(J_i) O_{l'}^{m'}(J_j) . \tag{1b}$$

The summation is over the two hexagonal sublattices. V_{ci} is the crystal field, which may qualitatively be described by the crystal-field parameters deduced by Rainford.[32] For a discussion of the origin of the general two-ion exchange term $\mathcal{H}_1'$,

see the article by Jensen *et al.*[33] The O_l^m are tensor operators working on the ground-state ($J=4$) multiplet. The coupling to phonons has been neglected, which may be justified by the fact that no anticrossing effects owing to phonon modes was observed in zero-magnetic field. In this analysis we shall also ignore the coupling between the excitations propagating on the hexagonal sites and the excitations propagating on the cubic sites, which have much higher energies.[5] A rough estimate[34] shows that the correction to the energies owing to this effect is only about 4%.

We now consider only the ground-state single $|0\rangle$ and the excited doublet $|x\rangle$, $|y\rangle$ and represent these states by an effective spin $S=1$. The Hamiltonian [Eqs. (1)] may easily be projected on to the basis spanned by these states. Ignoring the transitions within the doublet, which turn out to be unimportant to first order in the high-density expansion anyhow, the most general Hamiltonian may be written

$$\mathcal{H}=\sum_i \Delta(S_i^z)^2-\sum_{ij,\,\alpha\beta}\mathcal{J}_{ij}^{\alpha\beta}S_i^\alpha S_j^\beta\,, \tag{2}$$

where the higher-order terms in (1) with $m, m'=0, \pm 1$ have been effectively included in the resulting effective bilinear exchange coupling $\mathcal{J}_{ij}^{\alpha\beta}$, between spins i and j. Δ is the crystal-field splitting and α and β are Cartesian coordinates. The single-ion part of $\mathcal{H}$ is denoted by $\mathcal{H}_0$ and the two-ion part by $\mathcal{H}_{\rm int}$. The analysis of the temperature dependence of particular modes in the exciton spectrum gave the value $\Delta=3.2$ meV, which is in fair agreement with the value $\Delta=2.93$ meV obtained by Jensen[34] by analyzing the field dependence of the excitations at zero wave vector.

To calculate the magnetic excitation spectrum, it is convenient to introduce the Green's functions

$$G^{\alpha\beta}(\vec{r}_1,\tau_1;\vec{r}_2,\tau_2)=\langle T_\tau S^\alpha(\vec{r}_1,\tau_1)S^\beta(\vec{r}_2,\tau_2)\rangle\,, \tag{3}$$

where $\langle T_\tau\cdots\rangle$ denotes the thermal average of the τ-ordered product of operators in the interaction representation

$$S^\alpha(\vec{r},\tau)=e^{\mathcal{H}_0\tau}S^\alpha(\vec{r})\,e^{-\mathcal{H}_0\tau}\,. \tag{4}$$

The Green's functions are defined for $\alpha,\beta=x,y$ only. It is a standard procedure[35] to expand the Green's functions in the form

$$G^{\alpha\beta}(\vec{r}_1,\tau_1;\vec{r}_2,\tau_2)=\frac{\langle T_\tau S^\alpha(\vec{r}_1,\tau_1)S^\beta(\vec{r}_2,\tau_2)\,\mathcal{S}(\beta)\rangle_0}{\langle\mathcal{S}(\beta)\rangle_0}\,,$$
$$\mathcal{S}(\beta)=T_\tau\exp\left(-\int_0^\beta\mathcal{H}_{\rm int}(\tau)\,d\tau\right)\,. \tag{5}$$

The averages are taken with respect to $\mathcal{H}_0$. The corresponding noninteracting Green's functions are

$$G_0^{\alpha\beta}(\vec{r}_1,\tau_1;\vec{r}_2,\tau_2)=\langle T_\tau S^\alpha(\vec{r}_1,\tau_1)S^\beta(\vec{r}_2,\tau_2)\rangle_0$$
$$=g_0^{\alpha\alpha}(\vec{r}_1,\tau_1;\vec{r}_2,\tau_2)R\,\delta_{\alpha\beta}\,, \tag{6}$$

where

$$g_0^{\alpha\alpha}(\vec{r}_1,\tau;\vec{r}_2,0)=\{e^{\Delta|\tau|}[1+n(\Delta)]+e^{-\Delta|\tau|}n(\Delta)\}\,\delta_{12}\,, \tag{7a}$$

$$R=\langle(|0\rangle\langle 0|-|\alpha\rangle\langle\alpha|)\rangle=n_0-n_\alpha$$
$$=(1-e^{-\beta\Delta})(1+2e^{-\beta\Delta})^{-1}\,, \tag{7b}$$

and

$$n(\Delta)=(e^{\beta\Delta}-1)^{-1}\,. \tag{7c}$$

$g_0^{\alpha\alpha}$ is defined in the interval $-\beta<\tau<\beta$, and n_0 and n_α are Boltzmann population factors of the levels $|0\rangle$ and $|\alpha\rangle$. The Fourier components are defined in terms of the Matsubara frequencies $2n\pi/\beta$ in the usual way (n integer),

$$G^{\alpha\beta}(\vec{q},i\omega_n)=\sum_{\vec{r}_2}\int_0^\beta d\tau\,G^{\alpha\beta}(\vec{r}_1,\tau;\vec{r}_2,0)\,e^{i\vec{q}\cdot(\vec{r}_1-\vec{r}_2)}\,e^{i\omega_n\tau}\,, \tag{8a}$$

$$G'^{\alpha\beta}(\vec{q},i\omega_n)=\sum_{\vec{r}_2'}\int_0^\beta d\tau\,G^{\alpha\beta}(\vec{r}_1,\tau;\vec{r}_2',0)\,e^{i\vec{q}\cdot(\vec{r}_1-\vec{r}_2')}\,e^{i\omega_n\tau}\,. \tag{8b}$$

$\vec{r}_2$ denotes ions at the same sublattice as $\vec{r}_1$, and $\vec{r}_2'$ denotes the ions at the opposite sublattice. The inter- and intrasublattice exchange constants $\mathcal{J}^{\alpha\beta}(\vec{q})$ and $\mathcal{J}'^{\alpha\beta}(\vec{q})$ are defined in a similar way. The analytic continuation of the Green's functions $G^{(\prime)\alpha\beta}(\vec{q},i\omega_n)$ are related to the usual measured dynamical susceptibility by

$$\chi^{(\prime)\alpha\beta}(\vec{q},\omega)=g^2\mu_B^2G^{(\prime)\alpha\beta}(\vec{q},i\omega_n)\,,\quad i\omega_n\to\omega\,. \tag{9}$$

To zeroth order in $1/Z$ this formalism is exactly equivalent to the enhanced dynamical susceptibility formalism used by Holden and Buyers[36] to analyze the dynamics of the singlet-ground-state system Pr_3Tl. The Fourier transforms of the noninteracting Green's functions are

$$G_0(i\omega_n)=g_0(i\omega_n)R\,, \tag{10a}$$

where

$$g_0(i\omega_n)=2\Delta[\Delta^2-(i\omega_n)^2]^{-1}\,. \tag{10b}$$

The Green's functions $G^{\alpha\beta}(\vec{q},i\omega_n)$ are simple linear combinations of the correlation functions $K_{+-}(\vec{q},i\omega_n)$ defined by Vaks *et al.*[22] or of the Green's functions $G_{\alpha\beta,\gamma\delta}(\vec{q},i\omega_n)$ defined by Yang and Wang[25] in terms of standard basis operators. Hence, the rules for drawing and calculating diagrams can be inferred easily by applying the methods of these authors.

In general, the expansion (5) can be represented by a sum of connected diagrams representing an aggregate of single-cell blocks joined by interaction lines. The noninteracting Green's functions are represented by full lines, and the interactions by wavy lines. The propagators $G^{\alpha\beta}(\vec{q},i\omega_n)$ are represented by double lines. The single-cell blocks are surrounded by broken lines to denote that the propagators involved are restricted to the same site. A diagram containing N independent wave-vector

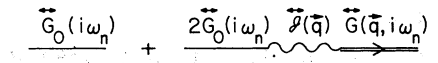

FIG. 2. RPA diagram representing the zeroth-order term in the $1/Z$ expansion.

labels, which are eventually summed over, is of order $(1/Z)^N$. The zeroth-order diagrams simply consist of noninteracting Green's functions connected with interaction lines (see the RPA diagrams in Fig. 2). The analytic expressions corresponding to these chain diagrams are

$$G^{\alpha\beta}(\vec{q}, i\omega_n) = G_0(i\omega_n)\delta_{\alpha\beta} + 2G_0(i\omega_n)\sum_\gamma \mathcal{J}^{\alpha\gamma}(\vec{q})G^{\gamma\beta}(\vec{q}, i\omega_n) + 2G_0(i\omega_n)\sum_\gamma \mathcal{J}'^{\alpha\gamma}(\vec{q})G'^{\gamma\beta}(\vec{q}, i\omega_n) , \quad (11a)$$

$$G'^{\alpha\beta}(\vec{q}, i\omega_n) = 2G_0(i\omega_n)\sum_\gamma \mathcal{J}'^{\alpha\gamma *}(\vec{q})G^{\gamma\beta}(\vec{q}, i\omega_n) + 2G_0(i\omega_n)\sum_\gamma \mathcal{J}^{\alpha\gamma}(\vec{q})G'^{\gamma\beta}(\vec{q}, i\omega_n) , \quad (11b)$$

or in matrix notation

$$\vec{\vec{G}}(\vec{q}, i\omega_n) = G_0(i\omega_n)\vec{\vec{1}} + 2G_0(i\omega_n)\vec{\vec{\mathcal{J}}}(\vec{q})\vec{\vec{G}}(\vec{q}, i\omega_n) , \quad (12)$$

where

$$\vec{\vec{G}}(\vec{q}, i\omega_n) = \begin{pmatrix} G^{xx}(\vec{q}, i\omega_n) & G^{xy}(\vec{q}, i\omega_n) & G'^{xx}(\vec{q}, i\omega_n) & G'^{xy}(\vec{q}, i\omega_n) \\ G^{yx}(\vec{q}, i\omega_n) & G^{yy}(\vec{q}, i\omega_n) & G'^{yx}(\vec{q}, i\omega_n) & G'^{yy}(\vec{q}, i\omega_n) \\ G'^{xx*}(\vec{q}, i\omega_n) & G'^{xy*}(\vec{q}, i\omega_n) & G^{xx}(\vec{q}, i\omega_n) & G^{xy}(\vec{q}, i\omega_n) \\ G'^{yx*}(\vec{q}, i\omega_n) & G'^{yy*}(\vec{q}, i\omega_n) & G^{yx}(\vec{q}, i\omega_n) & G^{yy}(\vec{q}, i\omega_n) \end{pmatrix} . \quad (13)$$

$\vec{\vec{\mathcal{J}}}(\vec{q})$ is defined in a completely analogous way. From Eq. (12) one sees immediately that $\vec{\vec{G}}(\vec{q}, i\omega_n)$ is diagonalized by the same unitary transformation that diagonalizes $\vec{\vec{\mathcal{J}}}(\vec{q})$. Denoting the eigenvalues of $\vec{\vec{\mathcal{J}}}(\vec{q})$ by $\mathcal{J}^N(\vec{q})$, $N=1, \ldots, 4$, and the eigenvalues of $\vec{\vec{G}}(\vec{q}, i\omega_n)$ by $G^N(\vec{q}, i\omega_n)$, we find the following solution to Eq. (12):

$$G^N(\vec{q}, i\omega_n) = \frac{g_0(i\omega_n)R}{1 - 2\mathcal{J}^N(\vec{q})g_0(i\omega_n)R} = 2\Delta R[(\omega_{\vec{q}}^N)^2 - (i\omega_n)^2]^{-1} , \quad (14)$$

where

$$(\omega_{\vec{q}}^N)^2 = \Delta^2 - 4\Delta R\mathcal{J}^N(\vec{q}) . \quad (15)$$

The poles of the Green's functions ω_q^N are the frequencies of the excitation modes within the random-phase approximation. The propagators of the four excitations are thus expressed directly in terms of the effective exchange interactions $\mathcal{J}^N(\vec{q})$.

The dispersion relations, measured in high-symmetry directions by Houmann *et al.*,[2] were least-squares fitted to the expression (15). The crystal-field splitting Δ was fixed at the previously determined value 3.2 meV. The two-ion part of the Hamiltonian was assumed to be

$$\mathcal{H}_{\rm int} = -\sum_{ij} \mathcal{J}_{ij}\vec{S}_i \cdot \vec{S}_j + \mathcal{J}_{ij}^{\rm AN} \times \{(\hat{R}_{ij} \cdot \vec{S}_i)(\vec{R}_{ij} \cdot \vec{S}_j) - \tfrac{1}{2}[(\hat{R}_{ij}^x)^2 + (\hat{R}_{ij}^y)^2](\vec{S}_i \cdot \vec{S}_j)\} , \quad (16)$$

where $\hat{R}_{ij}$ is the unit vector along $\vec{r}_i - \vec{r}_j$. This is the most general axial symmetric Hamiltonian in the form (2); it effectively includes electric and magnetic multipole terms, and also higher-order Kaplan-Lyons terms[37] originating from orbital contributions to the exchange interaction. The isotropic term $\frac{1}{2}[(R_{ij}^x)^2 + (R_{ij}^y)^2](\vec{S}_i \cdot \vec{S}_j)$ is included to ensure that $\mathcal{J}_{ij}^{\rm AN}$ has no influence on the degenerate modes at the zone center Γ. Exchange parameters for atoms out to fifth-nearest (100) plane (tenth-nearest neighbors) were included in the calculations of the Fourier transforms $\mathcal{J}^{\alpha\beta}(\vec{q})$ and $\mathcal{J}'^{\alpha\beta}(\vec{q})$. The resulting interatomic exchange parameters are given in Table I and the corresponding theoretical dispersion relations are shown in Fig. 1. Note that the fit is slightly better than the one presented in Ref. 31. The anisotropic part of the exchange interaction is generally of the same order of magnitude as the isotropic part. These exchange parameters reproduce all the main features of the spectrum correctly, so the resulting Fourier transforms $\mathcal{J}^{\alpha\beta}(\vec{q})$, to be used in higher-order calculations, are known with good accuracy, but too much physical significance should not be assigned to the particular interatomic exchange parameters. A physical description of the four branches is most conveniently given by considering the correlation functions of the spin operators corresponding to a mode with a given $\vec{q}$. These correlation functions can be calculated directly from the Green's functions. The Green's functions $G^{(\prime)\alpha\beta}(\vec{q})$ are easily determined by applying the inverse unitary transformation of that which diagonalized $\vec{\vec{\mathcal{J}}}(q)$ to the diagonal matrix with elements $\mathcal{J}^N(\vec{q})$.

The correlation functions are

$$S^{(\prime)\alpha\beta}(\vec{q}, \omega) = (1/\pi)(1 - e^{-\beta\omega})^{-1}\,{\rm Im}G^{(\prime)\alpha\beta}(\vec{q}, \omega) = (1 - e^{-\beta\omega})^{-1}\sum_N \frac{\Delta R}{\omega_q^N}\delta(\omega - \omega_{\vec{q}}^N)V_N^\alpha V_N^{\beta *} , \quad (17)$$

TABLE I. Interatomic exchange parameters as derived from the least-squares fit described in text. The positions of atoms are given in a coordinate system with x, y, and z axes in the a, b, and c directions, respectively.

Sublattice	Number of atoms	Coordinates of typical atom	Distance (Å)	$\mathcal{J}_{ij}$ (meV)	$\mathcal{J}_{ij}^{AN}$ (meV)
a	6	$(a,0,0)$	3.37	0.030	−0.084
a	6	$(0,\sqrt{3}a,0)$	6.36	−0.005	−0.033
a	6	$(a,\sqrt{3}a,0)$	7.35	0.009	−0.049
a	2	$(0,0,c)$	11.83	−0.052	0
a	12	$(a,0,c)$	12.39	0.025	0
b	6	$(0,-a/\sqrt{3},\frac{1}{2}c)$	6.28	−0.051	0.306
b	6	$(0,2a/\sqrt{3},\frac{1}{2}c)$	7.28	−0.013	−0.124
b	12	$(a,2a/\sqrt{3},\frac{1}{2}c)$	8.15	0.005	0.015
b	12	$(2a,-a/\sqrt{3},\frac{1}{2}c)$	9.67	0.010	−0.016
b	6	$(2a,2a/\sqrt{3},\frac{1}{2}c)$	10.34	0.005	0.021

where $\vec{V}_N=(V_N^x, V_N^y, V_N^{x'}, V_N^{y'})$ is the Nth eigenvector of $\vec{\mathcal{J}}(\vec{q})$ or $\vec{G}(\vec{q}, i\omega_n)$. The corresponding correlation functions in real space for a particular mode N with wave vector $\vec{q}$ and frequency ω_q^N are

$$\tfrac{1}{2}[\langle S^\alpha(\vec{r}_1,t)S^\beta(\vec{r}_2^{(\prime)},0)+S^\beta(\vec{r}_2^{(\prime)},0)S^\alpha(\vec{r}_1,t)\rangle]$$
$$=(1/N)[1-\exp(-\beta\omega_q^N)]^{-1}(\Delta R/\omega_q^N)$$
$$\times\tfrac{1}{2}\{V_N^\alpha V_N^{\beta(\prime)*}\exp[-i\vec{q}\cdot(\vec{r}_1-\vec{r}_2^{(\prime)})-i\omega_q^N t]$$
$$+V_N^{\beta(\prime)}V_N^{\alpha*}\exp[i\vec{q}\cdot(\vec{r}_1-\vec{r}_2^{(\prime)})+i\omega_q^N t]\}\,. \qquad (18)$$

Again, $\vec{r}_2$ is the position of a spin at the same sublattice as $\vec{r}_1$, and $\vec{r}_2'$ is a spin at the opposite sublattice.

For $\vec{q}$ in the b direction (y direction), where $\mathcal{J}^{xy}(\vec{q})$ and $\mathcal{J}'^{xy}(\vec{q})$ are zero, the polarization eigenvectors are of the form

$$V_x^{\pm}=(A^x, 0, \pm A^x e^{i\varphi^x}, 0)\,, \qquad (19a)$$
$$V_y^{\pm}=(0, A^y, 0, \pm A^y e^{i\varphi^y})\,. \qquad (19b)$$

These modes are longitudinal or transverse with linear polarizations. At the points Γ and M, the phases φ^x and φ^y are zero or π, so that the modes can be characterized exactly as optical or acoustic. An instantaneous picture of the modes at $q=0.25$ Å^{-1}, calculated on the basis of Eq. (18), is shown in Fig. 3. The optical longitudinal mode at this wave vector corresponds to the magnetic structure of neodymium, or of praseodymium with a few percent neodymium.[8] An interesting feature is that the phase φ^x passes through 90° at $\vec{q}\sim 0.85$ Å^{-1}, so that the mode which is optical at $\vec{q}=0$ eventually becomes acoustic at the point M. φ^x changes rapidly near M, which makes it difficult to connect the experimental points properly. In any case, the optical branches must be connected with the corresponding acoustic branches measured in the ΓKM direction at the point M, and acoustic and optical modes with the same polarization direction can not cross each other at any q value. The qualitative picture suggested by the present analysis is in agreement with all the measured points. However, even if our model fits the dispersion relations at low temperatures, the eigenvectors may be quite sensitive to the form of the exchange.

For $\vec{q}$ in the a direction (x direction), the polarization vectors V_N may be written

$$V_a=(D, iC, D, -iC)\,, \qquad (20a)$$
$$V_b=(A, iB, -A, iB)\,, \qquad (20b)$$
$$V_c=(B, -iA, -B, -iA)\,, \qquad (20c)$$
$$V_d=(C, -iD, C, +iD)\,, \qquad (20d)$$

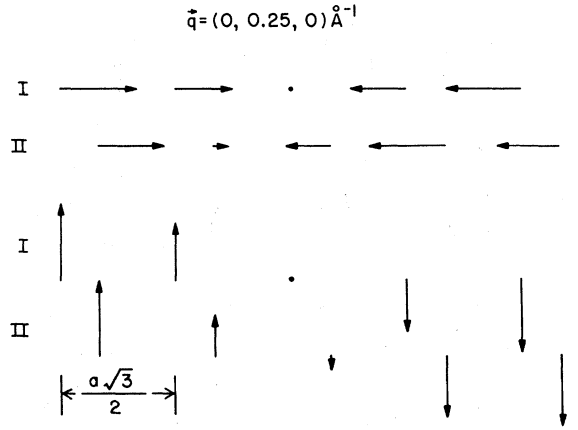

FIG. 3. Instantaneous picture of the two "acoustic" modes at $\vec{q}=0.25$ Å^{-1} in the b direction. The optical branches can be obtained by reversing the spins on one sublattice. The two sublattices are denoted I and II. Note that the magnetic moments on the two sublattices are not completely in phase.

where A, B, C, and D are real.

These modes are elliptically polarized with principal axes in the x and y directions. For the modes a and d, the x components of the spins on the two sublattices are in phase, and the y components are in antiphase, and for the modes b and c, the x components are in antiphase and the y components are in phase. Figure 4 shows an instantaneous picture of the spins as calculated on the basis of Eq. (18) for $q = 0.6$ Å^{-1}. At the point Γ, B and D are zero, so that the modes can be characterized as acoustic or optical with longitudinal or transverse polarization. Figure 5 shows the polarizations of the modes a and b at several q values in this direction. For both modes, the relative values of the axes of the ellipses changes rapidly in a complicated way for large q. At certain wave vectors, the modes are circularly polarized, which again might cause trouble in separating and identifying the modes experimentally. At the point M, the modes eventually become linear again. However, in agreement with the behavior in the Γ-M direction, the branch b,

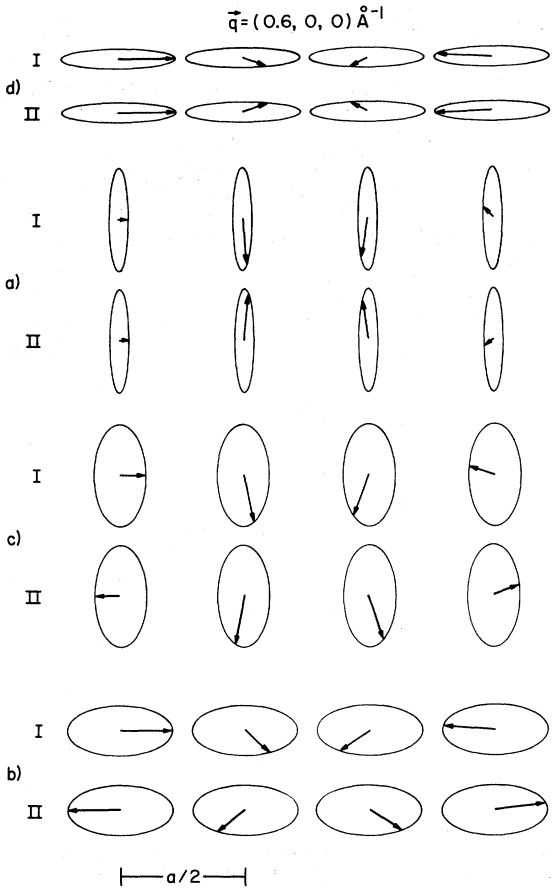

FIG. 4. Instantaneous picture of the four modes at $\vec{q} = 0.6$ Å^{-1} in the a-direction, as determined from the correlation functions $S^{\alpha\beta}(\vec{q}, \omega)$ and $S'^{\alpha\beta}(\vec{q}, \omega)$ calculated within the RPA. The two sublattices are denoted I and II.

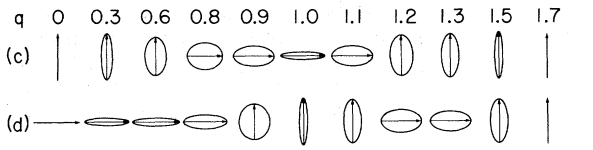

FIG. 5. Polarizations of the optical longitudinal and transverse modes calculated for several q values along the a direction. The two remaining modes can be obtained by rotating the ellipses in analogy with Fig. 4.

which at Γ corresponded to a longitudinal optical mode, now represents a transverse acoustic mode, whereas the optical transverse mode returns to its initial polarization, corresponding to the parameters A and D being zero at this point. The ellipticity of the modes is in agreement with the fact that the modes at finite $\vec{q}$ could not be extinguished completely by selecting the neutron-scattering vector $\vec{\kappa}$ parallel to the x or y direction.[38]

Thus, the RPA theory has allowed us to set up a theory of the dispersion relations, and to construct a complete model to describe the magnetic properties of the hexagonal ions. In Sec. III, we shall use this model to calculate the complete spectral function at any temperature and wave vector.

III. FLUCTUATION DAMPING OF MAGNETIC EXCITATIONS

In addition to a clear temperature dependence of the excitations in Pr, which could be completely accounted for within the random-phase approximation, Houmann *et al.*[2] observed a dramatic increase of the linewidth when the temperature was raised from 0.4 to 30 K. In this section we shall extend the $1/Z$ expansion one order beyond RPA using the exchange parameters derived in Sec. II. The formalism allows us to calculate the complete spectral function to this order without introducing any adjustable parameters.

The first-order corrections to the RPA Green's function $G^{\alpha\alpha}_{\mathrm{RPA}}(\vec{q}, i\omega_n)$ originate from the evaluation of the terms

$$\sum_{34} \mathcal{J}^{\gamma\delta}_{34} \langle T_\tau S^\alpha(\vec{r}_1, \tau_1) S^\alpha(\vec{r}_2, \tau_2) S^\gamma(\vec{r}_3, \tau_3) S^\delta(\vec{r}_4, \tau_4) \rangle_0 , \quad (21)$$

which occur in first order in the expansion (5). To calculate the diagrams giving rise to damping of excitations, we need only consider the terms corresponding to pairwise matching of the spin operators $S^\alpha(\vec{r}_1, \tau_1)$ and $S^\alpha(\vec{r}_2, \tau_2)$ with $S^\gamma(\vec{r}_3, \tau_3)$ and $S^\delta(\vec{r}_4, \tau_4)$, which are equal to

$$\sum_{34} \mathcal{J}^{\alpha\alpha}_{34} [g_0^{\alpha\alpha}(\vec{r}_1, \tau_1; \vec{r}_3, \tau_3) g_0^{\alpha\alpha}(\vec{r}_2, \tau_2; \vec{r}_4, \tau_4) + g_0^{\alpha\alpha}(\vec{r}_1, \tau_1; \vec{r}_4, \tau_4) g_0^{\alpha\alpha}(\vec{r}_2, \tau_2; \vec{r}_3, \tau_3)] \times \delta_{\alpha\gamma\delta} \langle (|0\rangle\langle 0| - |\alpha\rangle\langle\alpha|)_1 (|0\rangle\langle 0| - |\alpha\rangle\langle\alpha|)_2 \rangle_0 . \quad (22)$$

The temperature average over the diagonal operators is dependent on whether the site 1 is identical to or different from the site 2,

$$\langle(|0\rangle\langle 0| - |\alpha\rangle\langle\alpha|)_1(|0\rangle\langle 0| - |\alpha\rangle\langle\alpha|)_2\rangle_0 = R^2 + b\delta_{12} , \quad (23)$$

where $b = (5e^{-\beta\Delta} + e^{-2\beta\Delta})(1+2e^{-\beta\Delta})^{-2}$. The fact that this weight factor is not simply a product of the weight factors R associated with the noninteracting Green's functions invalidates the use of the original Dyson's equation in summing diagrams. The R^2 terms have already been taken into account via the RPA chain diagrams. The terms containing the factor $b\delta_{12}$ correspond to the single-cell block shown in the upper part of Fig. 6. The real part of the diagram gives rise to a small shift of the excitation energies. The imaginary part, which is of interest here, has the following analytic expression in ω_n, $\vec{q}$ space:

$$G_1^{\alpha\alpha}(i\omega_n) = 2g_0(i\omega_n)^2 bi \,\mathrm{Im}\frac{1}{N}\sum_{\vec{q}'} \mathcal{J}_S^{\alpha\alpha}(\vec{q}', i\omega_n) . \quad (24)$$

The summation over $\vec{q}'$ represents an effective dynamic "screened" *single-ion* interaction. $\mathcal{J}_S^{\alpha\alpha}(\vec{q}', i\omega_n)$ is defined self-consistently by the equation

$$\vec{\mathcal{J}}_S(\vec{q}', i\omega_n) = \vec{\mathcal{J}}(\vec{q}') + 2\vec{\mathcal{J}}(\vec{q}')[\vec{G}_0(i\omega_n) + \vec{G}_1(i\omega_n)]\vec{\mathcal{J}}_S(\vec{q}', i\omega_n), \quad (25)$$

which is represented by the chain diagram in Fig. 6. The corresponding sum over the *unscreened* exchange, $\mathcal{J}^{\alpha\alpha}(\vec{q}')$, is simply $\mathcal{J}_{ii}^{\alpha\alpha}$, which is zero per definition.

The matrices $\vec{\mathcal{J}}_S(\vec{q}', i\omega_n)$ and $\vec{G}_1(i\omega_n)$ are defined in analogy with Eq. (13). By grouping together terms with equivalent $\vec{q}'$ vectors in the summation in (24), one realized that $\mathcal{J}_S^{\alpha\alpha}(\vec{q}', i\omega_n)$ may be effectively replaced by $\frac{1}{2}[\mathcal{J}_S^{\alpha\alpha}(\vec{q}', i\omega_n) + \mathcal{J}_S^{\beta\beta}(\vec{q}', i\omega_n)]$, which is rotationally invariant. Therefore, the matrix $\vec{G}_1(i\omega_n)$ is proportional to the unit matrix, and the screened interaction $\vec{\mathcal{J}}_S(\vec{q}, i\omega_n)$ is diagonalized by the same unitary transformation which diagonalized $\vec{\mathcal{J}}(\vec{q}')$. The effective screened interactions for the four modes are thus

$$\mathcal{J}_S^N(\vec{q}', i\omega_n) = \mathcal{J}^N(\vec{q}')\{1 - 2\mathcal{J}^N(\vec{q})[G_0(i\omega_n) + G_1(i\omega_n)]\}^{-1} . \quad (26)$$

To get the effective interaction $[\mathcal{J}_S^{\alpha\alpha}(\vec{q}', i\omega_n) + \mathcal{J}_S^{\beta\beta}(\vec{q}', i\omega_n)]$ to be inserted in Eq. (24), the diagonal matrix with elements $\mathcal{J}_S^N(\vec{q}', i\omega_n)$ must be rotated according to the inverse unitary transformation. Because of the invariance of the trace under such a transformation we get

$$2[\mathcal{J}_S^{\alpha\alpha}(\vec{q}', i\omega_n) + \mathcal{J}_S^{\beta\beta}(\vec{q}', i\omega_n)] = \sum_N \mathcal{J}_S^N(\vec{q}', i\omega_n) . \quad (27)$$

Hence, the screened interaction in Eq. (24) finally turns out to be the average of the interactions $\mathcal{J}_S^N(\vec{q}', i\omega_n)$ determined from Eq. (26),

$$G_1(i\omega_n) = 2g_0(i\omega_n)^2 bi \frac{1}{N}\sum_{\vec{q}'}\frac{1}{4}\sum_N \mathrm{Im}\mathcal{J}_S^N(\vec{q}', i\omega_n) , \quad (28)$$

where the summation may be restricted to the irreducible part of the Brillouin zone. The diagram (Fig. 6) corresponds to scattering of excitation waves on single-site fluctuations of the population difference (or quadrupole moment), R. The intermediate states are magnetic excitations with wave vector $\vec{q}'$. This effect corresponds to scattering of spin waves on fluctuations of $\langle S^z\rangle$ for a simple ideal ferromagnet as discussed by Vaks *et al.*[22] It is interesting that the damping occurs to first order in the expansion. For boson or fermion systems, the lowest order imaginary part of the self-energy occurs in second order in the high-density expansion owing to interaction between excitations. In the present case the damping is of pure kinematic nature. The correction terms in Eq. (23) arise because the commutators of spin operators are operators, not simple numbers. The resulting diagonal Green's functions including *all* chain diagrams involving $G_0(i\omega_n)$ and $G_1(i\omega_n)$ are

$$G^N(\vec{q}, i\omega_n) = [G_0(i\omega_n) + G_1(i\omega_n)] \times\{1 - 2\mathcal{J}^N(\vec{q})[G_0(i\omega_n) + G_1(i\omega_n)]\}^{-1} . \quad (29)$$

The spectral functions, which are proportional to the neutron-scattering cross section, can easily be expressed in terms of the Green's functions using the fluctuation-dissipation theorem,

$$S^N(\vec{q}, \omega) = (1/\pi)(1 - e^{-\beta\omega})^{-1}\,\mathrm{Im}G^N(\vec{q}, \omega) . \quad (30)$$

Combining Eqs. (10), (28), (29), and (30) we find

$$S^N(\vec{q}, \omega) = \frac{1}{\pi}\frac{1}{1-e^{-\beta\omega}}\frac{\gamma(\omega)(\Delta^2 - \omega^2)}{[(\omega_q^N)^2 - \omega^2]^2 + [2\gamma(\omega)\mathcal{J}^N(\vec{q})]^2} , \quad (31)$$

where the damping parameter $\gamma(\omega)$ must be determined self-consistently by solving the integral equation

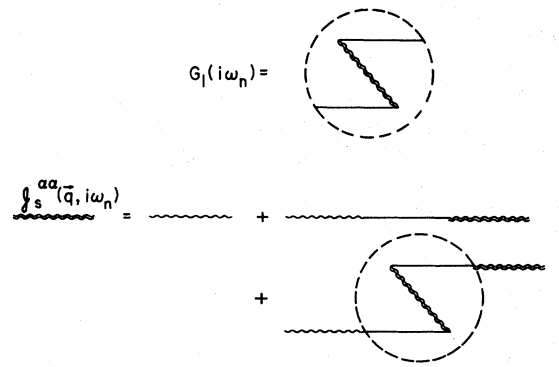

FIG. 6. First-order diagram representing fluctuation scattering of magnetic excitation waves. The double wavy lines represent "screened" interaction lines as defined by the diagram equation.

$$\gamma(\omega) = (\Delta^2 - \omega^2)\,\mathrm{Im}G_1^{\alpha\alpha}(\omega)$$

$$= 16\Delta^2 b \int_{\omega'} d\omega' \frac{\frac{1}{4}\sum_N N_T^N(\omega')\mathcal{J}^2(\omega')\gamma(\omega)}{(\omega'^2 - \omega^2)^2 + [2\gamma(\omega)\mathcal{J}(\omega')]^2} . \quad (32)$$

The summation over $\vec{q}'$ space has been changed to an integration over ω' space. $N_T^N(\omega)$ is the density of states for the N'th exciton mode at temperature T, and $\mathcal{J}(\omega')$ is the value of $\mathcal{J}^N(\vec{q}')$ for a mode with energy ω' determined by Eq. (15). This transformation is possible because $\mathcal{J}^N(\vec{q}')$ depends on $\vec{q}'$ only through ω'. Using Eq. (15) we get

$$N_T^N(\omega) = N_0^N(\omega(T=0))\omega(T=0)/\omega R , \quad (33)$$

where $\omega(T=0)$ is the zero-temperature RPA energy of the mode which has the energy ω at temperature T.

Using the parameters obtained from the least-squares fit in Sec. II, the averaged density of states $N_0(\omega)$ (Fig. 7) was determined by sampling more than 100 000 points in the irreducible part of the Brillouin zone. $N_0(\omega)$ is only very slightly sensitive to the goodness of the fit, as long as the main features of the dispersion relations were reproduced correctly. Once $N_0(\omega)$ is derived, the spectral function at any $\vec{q}$ vector and temperature is completely determined by Eqs. (31)–(33). The numerical solution of the integral equation (32) was performed as a computer iteration process. $N_0(\omega)$ has a very large peak around the crystal-field splitting Δ and is about a factor of 15 less at $\omega = 1.8$ meV corresponding to the zone center optical mode. Nevertheless, the damping is nearly constant for $1.5 < \omega < 2.8$ meV due to the factor $(\Delta^2 - \omega^2)$ or $\mathcal{J}(\omega)^2$, which increases rapidly when ω is removed away from Δ.

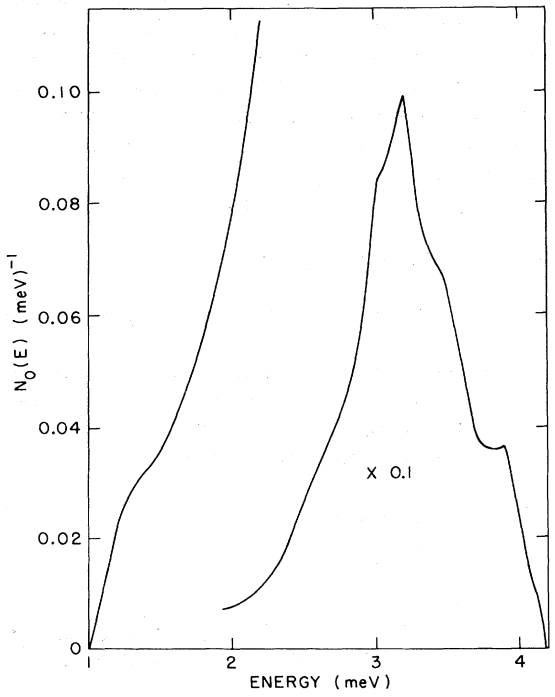

FIG. 7. Normalized density of states for the magnetic excitations in Pr. The curve was obtained by computer-smoothing the histogram calculated as described in text.

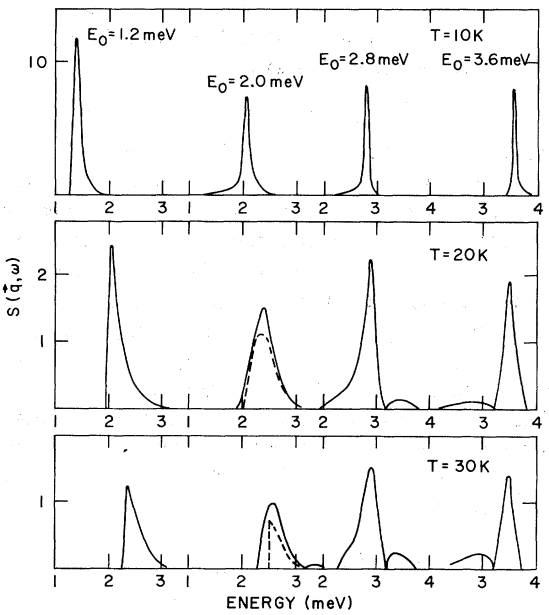

FIG. 8. Intrinsic line shapes of magnetic excitations in Pr calculated to first order in the high-density expansion. Solid lines: self-consistent line shapes determined using fully renormalized interaction propagators. Broken lines: line shapes calculated using RPA-screened propagators only. This approximation corresponds to omitting the last term of the lower diagram equation in Fig. 6. Note the different vertical scales at different temperatures.

Examples of intrinsic spectral functions at several energies and temperatures are shown in Fig. 8. At temperatures $\ll \Delta/k$, the line shapes approach Lorentzians with a full width at half-maximum of $8\pi b\Delta^2\mathcal{J}(\omega)^2 N_0(\omega)/\omega^2$, which vanishes like $e^{-\beta\Delta}$ as $T \to 0$ because of the factor b. However, already at $T = 10$ K there are marked deviations from this shape, and at higher temperatures the spectrum is highly distorted. The vanishing of the spectral function for $\omega = \Delta$ is due to the factor $\Delta^2 - \omega^2$. This effect will probably be removed by higher-order diagrams; in any case, it would be interesting to measure the spectral function with high resolution at several temperatures for a mode with energy around Δ.

Figure 8 also shows spectral functions calculated with a screened interaction $\mathcal{J}_S(\vec{q}')$, calculated without the last term of the diagrammatic equation in Fig. 6. In this case we have

$$\mathcal{J}_S^N(\vec{q}', i\omega_n) = \frac{\mathcal{J}_S^N(\vec{q}')[\Delta^2 - (i\omega_n)^2]}{(\omega_{\vec{q}}^N)^2 - (i\omega_n)^2} , \quad (34)$$

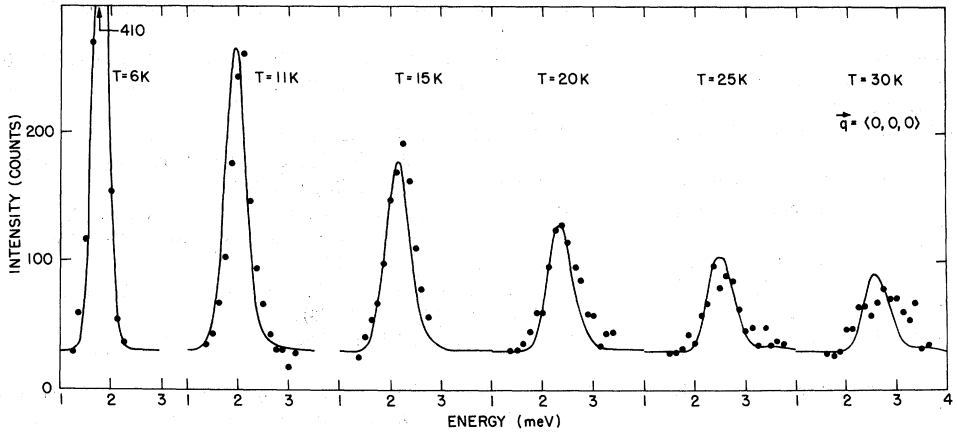

FIG. 9. Spectral functions for magnetic excitations in Pr. Points: neutron measurements (Ref. 38) and lines: self-consistently calculated line shapes convoluted with the experimental resolution (Gaussian, with full width at half-maximum 0.36 meV).

$$\mathrm{Im}\,\mathcal{J}_S^N(\vec{q}', \omega) = \frac{\pi \mathcal{J}_S^N(\vec{q}')(\Delta^2 - \omega^2)}{2\omega_{\vec{q}}^N}\left[\delta(\omega_{\vec{q}}^N - \omega) + \delta(\omega_{\vec{q}}^N + \omega)\right] . \tag{35}$$

Because of the δ function, $S^N(\vec{q}, \omega)$ vanishes for ω outside the exciton bands. This gives rise to a sharp cutoff of the intensity for modes with energies near the band edge, as pointed out by Stinchcombe.[30] Furthermore, the damping of the modes vanishes completely at high temperatures where the density of states approaches a δ function. However, the last term in Eq. (35) secures the self-consistency of the calculation and removes the above-mentioned singularities by effectively "smearing out" the density of states corresponding to the actual width of the modes. The theoretical line shapes convoluted with the experimental resolution function (Gaussian, full width at half-maximum = 0.36 meV), are compared with experiment in Fig. 9. The measured mode is the zone center optical mode with zero temperature energy $\omega_0 \sim 1.8$ meV. Almost complete agreement between positions of peaks, intensities, and line shapes is observed at any temperature. The agreement is least perfect at the highest temperatures, where the linewidth, as calculated to first order in the $1/Z$ expansion, is comparable to the energy as calculated to zeroth order. This indicates a slower convergence of the expansion, and we can expect higher-order corrections to the energies and linewidths to be important. However, statistical uncertainties of the measured points are important at $T \sim \Delta$ owing to the relatively small number of neutron counts.

IV. CONCLUSION

In Secs. II and III it has been shown that the spin dynamics of the magnetic excitations on the hexagonal sites of dhcp praseodymium can be understood in terms of the lowest order terms in a diagrammatic high-density expansion. The first-order RPA terms give an excellent description of the dispersion relations, as measured by inelastic neutron scattering, at any temperature. The analysis showed that the forces between the spins are highly anisotropic and of rather long range. However, no clear systematic behavior of the interatomic exchange constants, corresponding, for example, to the Ruderman-Kittel-Kasuya-Yosida interaction, was evident (Table I). The polarizations of the exciton modes are, in general, elliptic or linear, and the polarization vector changes rapidly as a function of $\vec{q}$, in particular, at large wave vectors.

The large damping of the excitations can be accounted for almost completely in terms of diagrams representing scattering of magnetic excitations on single-site fluctuations. Hence, damping effects due to other effects, such as interactions between excitations occurring to order $(1/Z)^2$ in the expansion, scattering on phonons, or direct Coulomb scattering with conduction electrons, can be entirely neglected at least at moderate temperatures. This fundamental understanding of the excitations in Pr may be valuable for the understanding not only of other singlet-ground-state systems of magnetic or nonmagnetic nature, such as the hydrogen bonded ferroelectrics,[39] but also of more complicated systems, since the formalism can easily be extended to arbitrary level schemes.[25]

An interesting feature is the fact that praseodymium with very small amounts of neodymium orders magnetically at low temperatures.[8] Inelastic neutron-scattering measurements of the dynamics in such systems will probably give important information on the dynamics in singlet-ground-state systems in the critical regime, and may provide a crucial test to the validity of the present theory in this regime.

ACKNOWLEDGMENTS

I am much indebted to J. C. G. Houmann and A. R. Mackintosh for communicating their neutron-diffraction data prior to publication. I would like to thank J. Jensen, M. Blume, V. J. Emery, D. Mukamel, and S. Krinsky for numerous illuminating discussions.

*Work supported by Energy Research and Development Administration.

[1]For a review on singlet-ground-state magnetism see B. R. Cooper, in *Magnetic Properties of Rare Earth Metals*, edited by R. J. Elliot (Plenum, London, 1972), p. 17; R. J. Birgeneau, AIP Conf. Proc. 10, 1664 (1973).

[2]J. G. Houmann, M. Chappelier, A. R. Mackintosh, P. Bak, O. D. McMasters, and K. A. Gschneider, Jr., Phys. Rev. Lett. 34, 587 (1975).

[3]K. A. McEwan, G. J. Cock, L. W. Roeland, and A. R. Mackintosh, Phys. Rev. Lett. 30, 287 (1973).

[4]T. Johansson, B. Lebech, M. Nielsen, H. Bjerrum-Møller, and A. R. Mackintosh, Phys. Rev. Lett. 25, 524 (1970).

[5]B. D. Rainford and J. G. Houmann, Phys. Rev. Lett. 26, 1254 (1971); 27, 223E (1971).

[6]R. M. Nicklow, N. Wakabayashi, M. K. Wilkinson, and R. E. Reed, Phys. Rev. Lett. 27, 334 (1971).

[7]R. J. Birgeneau, J. Als-Nielsen, and E. Bucher, Phys. Rev. B 6, 2724 (1972).

[8]B. Lebech, K. A. McEwen, and P. A. Lindgaard, J. Phys. C 7, 1684 (1975).

[9]T. Murao, J. Phys. Soc. Jpn. 31, 683 (1971).

[10]Y. Y. Hsieh and M. Blume, Phys. Rev. B 6, 2684 (1972).

[11]S. R. P. Smith, J. Phys. C 5, L157 (1972).

[12]I. Peschel, M. Klenin, and P. Fulde, J. Phys. C 5, L194 (1972).

[13]G. D. Houston and H. C. Boulton, J. Phys. C 4, 2097 (1971).

[14]B. Grover, Phys. Rev. A 140, 1944 (1965).

[15]B. R. Cooper, Phys. Rev. B 6, 2730 (1972).

[16]W. J. L. Buyers, T. M. Holden, E. C. Svensson, R. A. Cowley, and M. T. Hutchings, J. Phys. C 4, 2139 (1971).

[17]Y. L. Wang and B. R. Cooper, Phys. Rev. 185, 696 (1969).

[18]D. A. Pink, J. Phys. C 1, 1246 (1968); Phys. Rev. Lett. 33, 897 (1974).

[19]T. Murao and T. Matsubara, J. Phys. Soc. Jpn. 25, 352 (1968).

[20]M. Blume and J. Hubbard, Phys. Rev. B 1, 3815 (1970).

[21]M. A. Moore and H. C. W. L. Williams, J. Phys. C 5, 3185 (1972).

[22]V. G. Vaks, A. I. Larkin, and S. A. Pikin, Zh. Eksp. Teor. Fiz. 53, 281 (1967); 53, 1089 (1967) [Sov. Phys.-JETP 26, 188 (1968); 26, 647 (1968)].

[23]M. P. Kashchenko, N. F. Balakhonov, and L. V. Kurbatov, Zh. Eksp. Teor. Fiz. 64, 391 (1973) [Sov. Phys.-JETP 37, 201 (1973)].

[24]Yu. A. Izyumov and F. A. Kassan-Ogly, Fiz. Met. Metalloved. 30, 225 (1970).

[25]D. H-Y. Yang and Y-L. Wang, Phys. Rev. B 10, 4714 (1974).

[26]S. B. Haley and P. Erdös, Phys. Rev. B 5, 1106 (1972).

[27]H-G. Purwins, J. G. Houmann, P. Bak, and E. Walker, Phys. Rev. Lett. 31, 1585 (1973).

[28]P. Bak, AIP Conf. Proc. 24, 152 (1975).

[29]R. B. Stinchcombe, G. Horwitz, F. Englert, and R. Brout, Phys. Rev. 130, 155 (1963).

[30]R. B. Stinchcombe, J. Phys. C 6, 2484 (1973).

[31]P. Bak, Phys. Rev. Lett. 34, 1230 (1975).

[32]B. D. Rainford, AIP Conf. Proc. 5, 591 (1972).

[33]J. Jensen, J. G. Houmann, and H. Bjerrum Møller, Phys. Rev. B 12, 303 (1975).

[34]J. Jensen (private communications).

[35]A. H. Abrikosov, L. P. Gorkov, and I. E. Dzyaloshinski, *Methods of Quantum Field Theory in Statistical Physics* (Prentice-Hall, Englewood Cliffs, N. J., 1963).

[36]T. M. Holden and W. J. L. Buyers, Phys. Rev. B 9, 3797 (1974).

[37]T. A. Kaplan and D. H. Lyons, Phys. Rev. 129, 2072 (1963).

[38]J. G. Houmann and A. R. Mackintosh (private communications).

[39]For a list of systems, which may be described by singlet-ground-state Hamiltonians, see R. B. Stinchcombe [J. Phys. C 5, 2459 (1973)].